Chemical Science

ROYAL SOCIETY OF CHEMISTRY

EDGE ARTICLE

View Article Online
View Journal | View Issue

Cite this: *Chem. Sci.*, 2023, **14**, 6095

All publication charges for this article have been paid for by the Royal Society of Chemistry

Role of supramolecular polymers in photo-actuation of spiropyran hydrogels†

Chuang Li, ‡[ab] Qinsi Xiong, ‡[d] Tristan D. Clemons,[bd] Hiroaki Sai, [be] Yang Yang,[b] M. Hussain Sangji,[bf] Aysenur Iscen, §[bc] Liam C. Palmer, [bdh] George C. Schatz *[cd] and Samuel I. Stupp *[bdefgh]

Supramolecular-covalent hybrid polymers have been shown to be interesting systems to generate robotic functions in soft materials in response to external stimuli. In recent work supramolecular components were found to enhance the speed of reversible bending deformations and locomotion when exposed to light. The role of morphology in the supramolecular phases integrated into these hybrid materials remains unclear. We report here on supramolecular-covalent hybrid materials that incorporate either high-aspect-ratio peptide amphiphile (PA) ribbons and fibers, or low-aspect-ratio spherical peptide amphiphile micelles into photo-active spiropyran polymeric matrices. We found that the high-aspect-ratio morphologies not only play a significant role in providing mechanical reinforcement to the matrix but also enhance photo-actuation for both light driven volumetric contraction and expansion of spiropyran hydrogels. Molecular dynamics simulations indicate that water within the high-aspect-ratio supramolecular polymers exhibits a faster draining rate as compared to those in spherical micelles, which suggests that the high-aspect-ratio supramolecular polymers effectively facilitate the transport of trapped water molecules by functioning as channels and therefore enhancing actuation of the hybrid system. Our simulations provide a useful strategy for the design of new functional hybrid architectures and materials with the aim of accelerating response and enhancing actuation by facilitating water diffusion at the nanoscopic level.

Received 23rd January 2023
Accepted 14th May 2023

DOI: 10.1039/d3sc00401e

rsc.li/chemical-science

Introduction

Many complex biological functions are enabled by highly ordered structures that are organized through both covalent and supramolecular interactions. Iconic examples include deoxyribonucleic acid (DNA), a covalent biopolymer composed of a series of nucleotides, that can form the double helical structure known as DNA duplex through non-covalent base-pairing and thus encode the genetic information of life.[1,2] Another example is the sarcomere of skeletal muscle that integrates covalent titin with supramolecular polymers including actin and myosin to form the highly aligned contractile unit of a muscle fiber.[3,4] Those examples in nature have recently inspired increasing interest in the development of hybrid bonding polymers in which the supramolecular structure allows dynamics and reconfiguration while the covalent polymer offers mechanical robustness.[5–10] Multiple supramolecular interactions such as hydrogen bonding,[11–14] host–guest interactions,[15,16] electrostatic attraction,[17,18] among others have been integrated with covalent bonds to create supramolecular-covalent hybrid materials[19] for applications such as photocatalysis,[20] tough hydrogels,[21–23] tissue adhesives,[24,25] recyclable polyureas,[26] artificial muscles,[9,27] and soft robotics.[10] Importantly, supramolecular and covalent polymers can be integrated

[a]*Department of Polymer Science and Engineering, University of Science and Technology of China, Hefei, Anhui 230026, China*
[b]*Center for Bio-inspired Energy Science, Northwestern University, 2145 Sheridan Road, Evanston, IL 60208, USA*
[c]*Department of Chemical and Biological Engineering, Northwestern University, 2145 Sheridan Road, Evanston, IL 60208, USA. E-mail: g-schatz@northwestern.edu*
[d]*Department of Chemistry, Northwestern University, 2145 Sheridan Road, Evanston, IL 60208, USA. E-mail: s-stupp@northwestern.edu*
[e]*Department of Materials Science and Engineering, Northwestern University, 2220 Campus Drive, Evanston, IL 60208, USA*
[f]*Department of Biomedical Engineering, Northwestern University, 2145 Sheridan Road, Evanston, IL 60208, USA*
[g]*Department of Medicine, Northwestern University, 676 N St. Clair, Chicago, IL 60611, USA*
[h]*Simpson Querrey Institute, Northwestern University, 303 E. Superior Street, Chicago, IL 60611, USA*

† Electronic supplementary information (ESI) available: Experimental procedures, compound characterization and coarse-grained simulations including Supporting Fig. S1–S24, Supporting Tables S1 and S2. See DOI: https://doi.org/10.1039/d3sc00401e

‡ These authors contributed equally to this work.

§ Present address: Max Planck Institute for Polymer Research, Ackermannweg 10, Mainz 55128, Germany.

into a single material through either a simultaneous[5] or sequential polymerization strategy,[9,10] and interactions among both components makes it possible to precisely tune the dynamics and robustness of the hybrid material.[28]

An important knowledge gap in the development of supramolecular-covalent hybrid materials is the role of morphology in the supramolecular component. In living systems, there are many examples in which the shape of the supramolecular component plays a critical role in their highly dynamic and complex functions.[29] For example, the fibrous network of the cytoskeleton provides mechanical support and helps cells maintain their shape and internal organization.[30,31] The spherical shape of many organelles such as lysosomes helps degrade parts of cells and destroy invading viruses and bacteria.[32] Synthetic supramolecular polymers[33–36] alone have been demonstrated to self-assemble into structures that exhibit many different morphologies including micelles,[37,38] fibers,[39–42] ribbons,[43–45] tubes,[46–49] among others, but only very few examples have been reported in which the shapes of supramolecular components are considered when integrated with covalent systems.[9,20] Peptide amphiphiles (PA) are versatile self-assembling building blocks to create designable supramolecular morphologies[50] and we recently reported that fibrous PA supramolecular polymers act as a dynamic water-draining skeleton that enhances the photo-contraction performance of the hybrid materials.[10] We also reported a covalent hydrogel containing photo-expanding spiropyran (SP) photo-switches that displayed a volumetric swelling (rather than contraction) upon light irradiation.[51] However, hybrid materials based on this photo-expanding system have not been demonstrated. We report here on the molecular design of light-responsive hybrid hydrogels through the incorporation of supramolecular components with variable self-assembled shapes into covalent photo-expanding as well as photo-contracting systems. We systematically investigate the critical functional roles of the supramolecular assemblies through both experimental and computational studies.

Results and discussion

Design of PAs with variable supramolecular morphologies

To create a chemical connection with the covalent network, we synthesized supramolecular monomer **PA 1** (Fig. 1A) that contains a polymerizable methacrylamide group at the amino terminus (N terminus; C_{16}VVEEK-methacrylamide), which self-assembled into ribbon-shaped supramolecular polymers (Fig. S1†). The noncovalent polymerization of **PA 1** and unfunctionalized **PA 2** (C_{16}VVEE-NH_2) with a molar ratio of 1 : 1 in aqueous solution was found to form high-aspect-ratio twisted supramolecular ribbons. Cryogenic transmission electron microscopy (cryo-TEM, Fig. 1D) and atomic force microscopy (AFM, Fig. 1G) revealed that the co-assembled supramolecular filaments are several microns in length and tens of nanometers in diameter. Small-angle X-ray scattering (SAXS) curves have a slope of −1.3 at low q, which further indicated the formation of high-aspect-ratio filaments (Fig. 1J). We changed the order of hydrophobic valines and hydrophilic glutamic acids in **PA 1** and **PA 2**, and synthesized **PA 3** (C_{16}VEVEK-methacrylamide) and **PA 4** (C_{16}VEVE-NH_2) in order to connect to a covalent network. These supramolecular copolymers also formed high-aspect-ratio fibers (Fig. 1B, E, H and K). In order to obtain different supramolecular morphologies, we also designed PAs which replace the two hydrophobic valines with hydrophilic glutamic acids, resulting into polymerizable **PA 5** (C_{16}EEEEK-methacrylamide) and unfunctionalized **PA 6** (C_{16}EEEE-NH_2). The co-assembly of **PA 5** and **PA 6** (Fig. 1C) with a molar ratio of 1 : 1 was found to form spheres with polydispersity in size by cryo-TEM (Fig. 1F) and atomic force microscopy (AFM) (Fig. 1I). As expected SAXS scattering scans shown in Fig. 1L reveal completely flat with a slope of 0 for q in the range 0.05–0.1 $Å^{-1}$, confirming the formation of low-aspect-ratio spherical structures. Dynamic light scattering (DLS) indicated that the diameter of these micellar aggregates is approximately 50.7 nm (Fig. S2†). These results demonstrate that we could obtain different supramolecular morphologies in the co-assemblies investigated by simply changing peptide sequences.

Synthesis of supramolecular-covalent hybrid hydrogel

Co-assembled supramolecular nanostructures that contain polymerizable methacrylamide groups were used for free-radical copolymerization in the presence of *N*-isopropylacrylamide (NIPAM) and methacrylate-spiropyran monomers, *N*,*N*′-methylenebisacrylamide (MBAAm) cross-linkers, and ammonium persulfate and tetramethylethylenediamine initiators (Table S1†). The connection between supramolecular polymers and the covalent network creates a "hybrid bonding polymer" which our previous work showed is critical for mechanical reinforcement of the resulting hydrogels.[6,10] Using rheological measurements, we investigated how the shape of the supramolecular nanostructure affects the mechanical properties (Fig. 2A). We found that the presence of supramolecular nanostructures with high-aspect-ratio morphologies (VVEE or VEVE) resulted in a significant mechanical reinforcement of the hybrid hydrogel and the reinforcement is tunable by adjusting the weight percentage of the high-aspect-ratio supramolecular components (Fig. 2B and C). We suggest the observed reinforcement can be explained by the covalent connection as well as physical entanglement among supramolecular high-aspect-ratio fibers or ribbons and covalent polymers. In contrast, the micellar supramolecular structures were found to provide a minimal contribution to mechanical reinforcement of the hybrid materials even though the weight percentage was as high as 2 wt% (Fig. 2D). This could be attributed to the fact that the supramolecular micelles have nearly no entanglement interactions with the covalent polymers given their spherical shape. These results demonstrate that the shape of the supramolecular nanostructures is critical for the mechanical reinforcement of these hybrid materials.

Photoisomerization of supramolecular-covalent hybrid hydrogels

In addition to mechanical reinforcement, the supramolecular nanostructures were also found to play an important role in the

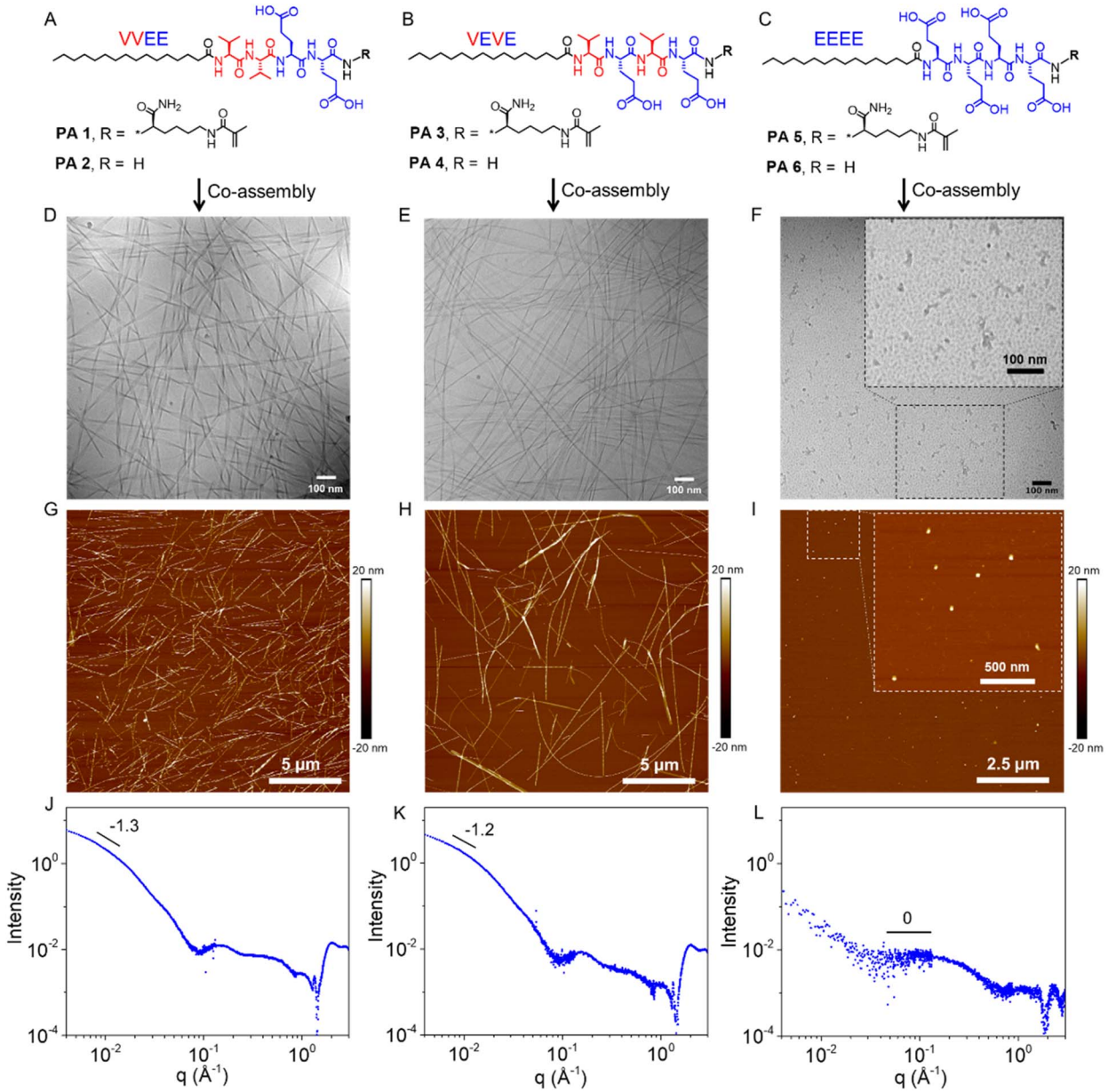

Fig. 1 (A–C) Chemical structure of PAs. (D and E) A representative cryo-TEM image of high-aspect-ratio morphologies formed by co-assembly with a molar ratio of 1 : 1 of **PA 1** and **PA 2** (ribbons, D), **PA 3** and **PA 4** (fibers, E). Scale bar is 100 nm. (F) A representative cryo-TEM image of spherical micelles formed by co-assembly of **PA 5** and **PA 6** with a molar ratio of 1 : 1. (G and H) A representative AFM image of high-aspect-ratio morphologies formed by co-assembly with a molar ratio of 1 : 1 of **PA 1** and **PA 2** (G), **PA 3** and **PA 4** (H). (I) A representative AFM image of spherical micelles formed by co-assembly of **PA 5** and **PA 6** with a molar ratio of 1 : 1. (J and K) SAXS profiles of co-assembly in water with a molar ratio of 1 : 1 of **PA 1** and **PA 2** (J), **PA 3** and **PA 4** (K), **PA 5** and **PA 6** (L), showing the background-subtracted scattered intensity *versus* the scattering vector *q* (log–log plot).

photoisomerization of the hybrid hydrogels containing spiropyran compounds **C1** and **C2** (Fig. 3A and S3†). Our previous study showed that the pure covalent spiropyran hydrogels displayed a volume contraction (for **C1**) and expansion (for **C2**), respectively, upon light irradiation due to the isomerization of the protonated merocyanine (MC) to SP.[51] We found that the hybrid hydrogels (VVEE, VEVE and EEEE) exhibited the same trend in terms of in volume change as do the pure covalent spiropyran hydrogels upon irradiation (Fig. 3B), indicating the presence of supramolecular components does not inhibit the observed chemically driven photo-contraction or photo-expansion. The light-induced volume change of the EEEE hybrid was found to be slightly larger than that of the VVEE or VEVE hybrids, which we attribute to the fact that the EEEE hybrid is mechanically softer (Fig. S4†) and has a relatively loose crosslinked network. This trend was also verified in the pure covalent hydrogels, where samples with a lower crosslinking density displayed a larger volume change (Fig. S5†).

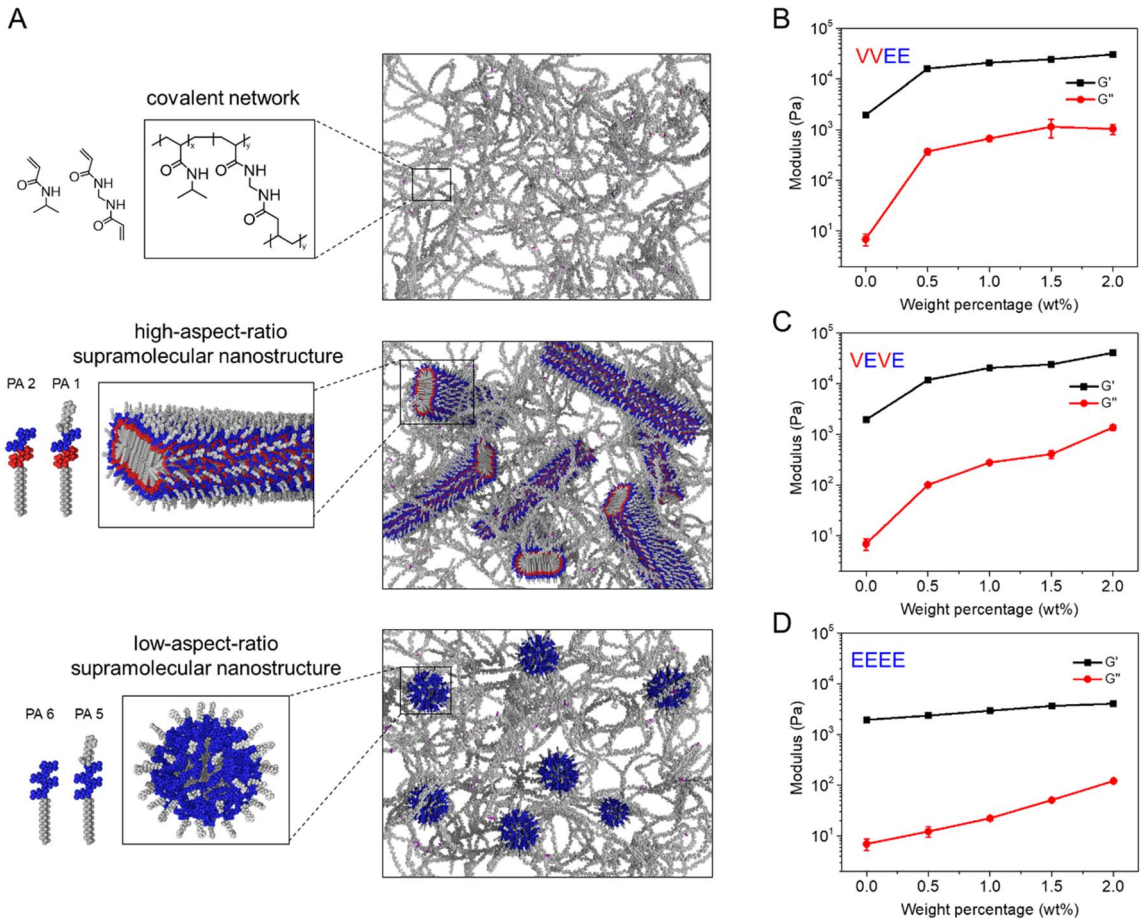

Fig. 2 (A) Molecular graphics representation of supramolecular-covalent hybrid polymers formed through a free-radical polymerization process in the presence of the high-aspect-ratio (VVEE or VEVE, middle) or low-aspect-ratio spherical (EEEE, bottom) supramolecular nanostructures. The covalent network without supramolecular nanostructures is shown at the top. (B–D) Storage and loss moduli of hybrid hydrogels with variable content of total PA from 0 wt% to 2.0 wt%, with a fixed co-assembly ratio at 1 : 1 (molar ratio of methacrylate PA to unfunctionalized PA) of **PA 1** and **PA 2** (B), **PA 3** and **PA 4** (C), **PA 5** and **PA 6** (D).

In order to gain more insight into the mechanisms underlying the photo-actuation behavior, we performed a series of molecular dynamics (MD) simulations on the hybrid systems using the coarse-grained (CG) martini force field (see Fig. S6–S8† for details on the martini beads and initial conformations). Hybrid systems with supramolecular high-aspect-ratio nanostructures (VVEE hybrid; VEVE was not investigated due to its similarity to VVEE hybrid) or supramolecular spherical micelle nanostructures (EEEE hybrid) containing **C1** and **C2** were simulated over a time scale of approximately 2 μs (Table S2†). Control systems (pure covalent polymers without supramolecular components) with different crosslinking densities were also investigated using the same simulations. Snapshots of the final structures simulated shown in Fig. 3C, D and S9† indicated that VVEE and EEEE hybrids maintained their supramolecular high-aspect-ratio filaments and spherical micelle nanostructures, respectively, regardless of whether the spiropyran is in its SP or protonated merocyanine (MC) form. Interestingly, while maintaining their original high-aspect-ratio or spherical morphology, the internal PA nanostructures all undergo some degree of deformation, especially the PAs in the VVEE hybrid systems, which all transformed from the original cylindrical fibers to twisted fibers (see Fig. S10 and S11†). Due to the presence of these supramolecular nanostructures and their chemical connection to the covalent polymers, the pre-stretched covalent polymers collapsed around the internal PA nanostructures. We calculated the average number of spiropyran moieties interacting with each other within each polymer chain (contact number) to understand how interactions affect the photoisomerization process. As shown in Fig. 3E and S12,† the contact number increased in systems containing **C1** but decreased in systems containing **C2** upon irradiation. This suggests that irradiation leads to the formation of small spiropyran clusters in systems containing **C1**, while spiropyran units do not form clusters upon irradiation in systems containing **C2**, which should be a result of repulsive electrostatic interactions. We note that the average contact numbers are never much larger than 1, so clustering leading to a phase transition is probably not an important factor in the isomerization. The opposite trend between **C1** and **C2** systems was also observed in calculations of the solvent accessible surface area (SASA, Fig. 3F) and in values of the coordination number

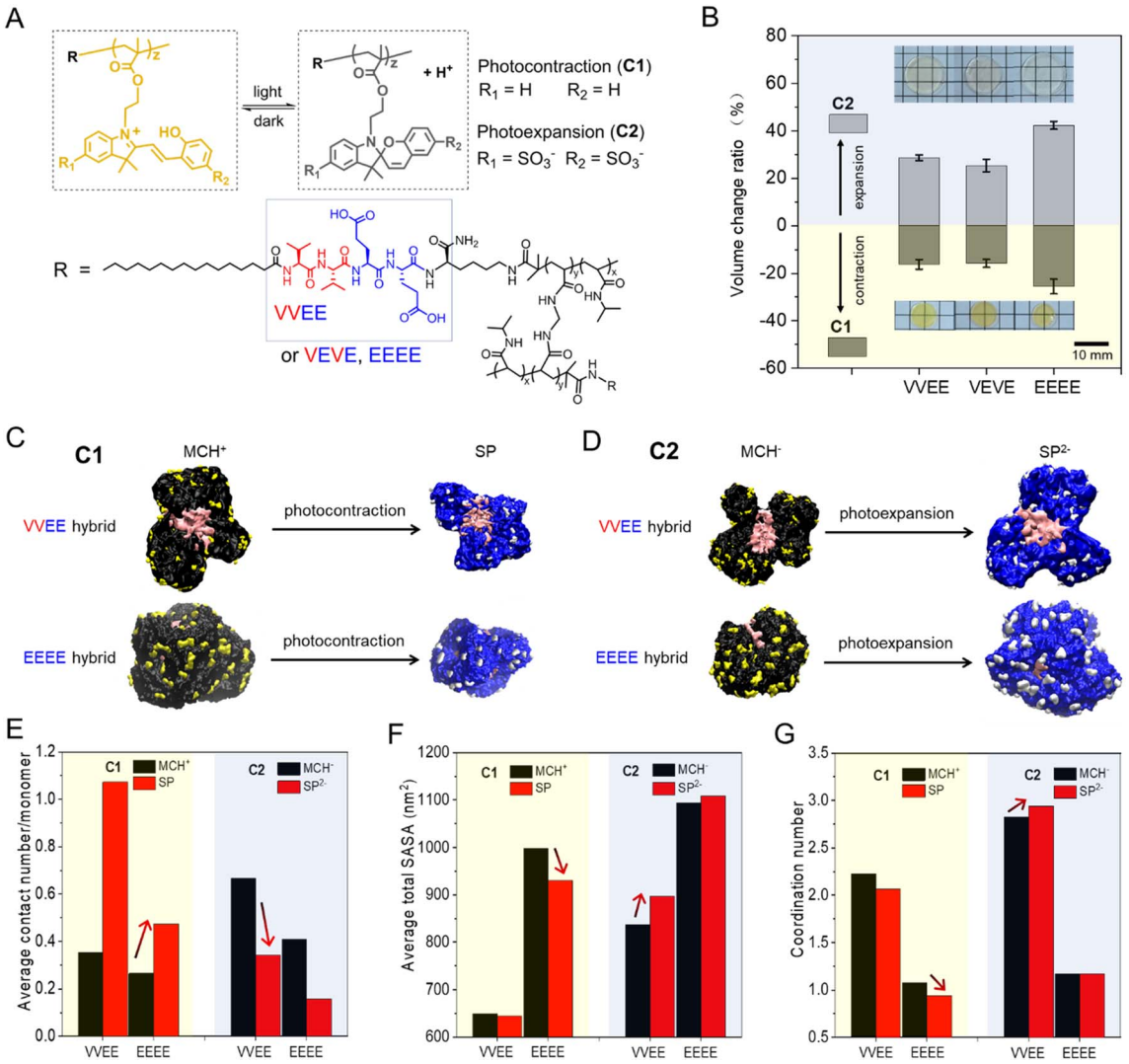

Fig. 3 (A) Chemical structures of VVEE, VEVE and EEEE hybrid PNIPAM polymers containing photo-switches **C1** and **C2** in their spiropyran (right) and merocyanine (left) forms. (B) Plot of the net volume change of different hydrogels upon irradiation (insets show photographs of **C2** expanding (top) and **C1** contracting (bottom) hydrogels after irradiation). (C and D) Snapshots of final simulated structures of VVEE (top) and EEEE (bottom) hybrid polymers containing **C1** (C) and **C2**; MCH form-PNIPAM is shown in black, SP form-PNIPAM in blue; PA assemblies in pink; MCH molecules in yellow; SP moieties in gray. (E) Average MCH or SP contacts involved within each polymer chain containing **C1** (left) and **C2** (right) two MCH (or SP) neighbors form a contact if their interatomic separation is shorter than 0.7 nm. (F) Average value of the solvent accessible surface area (SASA) for the total polymer systems containing **C1** (left) and **C2** (right). (G) Coordination number of water beads found in the first solvation shell of radial distribution functions (data in (E–G) were averaged over the last 200 ns of each simulation and arrows in (E–G) indicate value changes in the *y* axis).

between the polymers and solvent particles (Fig. 3G) (see second set of simulations in Fig. S13†). These observed trends above could be explained as arising from a decrease in the net charge density of **C1** upon irradiation, which results in less repulsive electrostatic interactions among SPs and consequently a higher contact number, less interaction between polymers and water, and a net photo-contraction of the hydrogel. However, the net charge density of **C2** increased upon irradiation and therefore exhibited an opposite trend *versus* **C1**. These results suggest that the photoinduced decrease (or increase) of charge density accelerates the drainage of water out of (or into) the gel (Fig. S14 and S15†), which agrees with the volume changes we observed experimentally. Collectively, these results indicate that the addition of sulfonate groups in **C2** can trigger an opposite photo-actuation behavior relative to **C1**, and most importantly, the presence of supramolecular nanostructures in the hybrid systems does not inhibit the photoisomerization of spiropyrans or the photo-actuation of SP hydrogels as we have observed in the covalent systems.[51]

Effect of supramolecular morphology on photo-contraction of the C1 hydrogels

To test photo-contraction performance, **C1** hydrogel thin films (0.5 mm thick) were cut into a cross shape (each arm 7.0 mm

long and 3.0 mm wide) and irradiated with light from the top (Fig. 4A). Because of the creation of a light-induced photo-isomerization gradient through the films, the films gradually bent up towards the direction of the light source. Eventually the films flattened as prolonged irradiation eliminated the isomerization gradient (Fig. 4B). Bending angles of the different thin films were measured during this bending-flattening process and plotted in Fig. 4C. It was found that the hybrid systems containing the high-aspect-ratio supramolecular morphology (VVEE and VEVE) exhibit the fastest response to light and give a maximum bending angle of ~70°. In contrast, hybrid materials containing the spherical micelle supramolecular morphology (EEEE) displayed a smaller bending angle (~44°), close to that of the soft covalent polymer control material (~33°), probably due to their low moduli. However, the stiff covalent polymer control sample with a higher crosslinking density exhibited a modulus and a maximum bending angle both close to that of the VVEE or VEVE hybrids, but bending of this highly crosslinked material was about 1.7 times slower (Fig. S16A and B†). These results indicated that mechanical enhancement by simply increasing covalent crosslinking density indeed contributes to the greater maximum bending angle of these hydrogels, but in turn limits the photoactuation rate because the denser network hinders water diffusion. The presence of high-aspect-ratio supramolecular polymer reinforces the hybrid hydrogels by physical entanglement and simultaneously maintains a relatively loose crosslinked network that is highly permeable to water, resulting in both a larger bending angle and a faster actuation rate. The results also demonstrate that the high-aspect-ratio supramolecular polymer is more effective than spherical aggregates in enhancing the mechanical properties as well as the photo-actuation performance of the hybrid system.

To gain further insight into the role of different supramolecular morphologies in photo-actuation, we carried out MD simulations and monitored changes in the concentration of trapped water for different hybrid systems before and after light irradiation. These are plotted on a logarithmic scale in Fig. 4D (see Methods for details). After fitting the slopes of all the curves plotted in Fig. 4D, we determined the draining rate of the

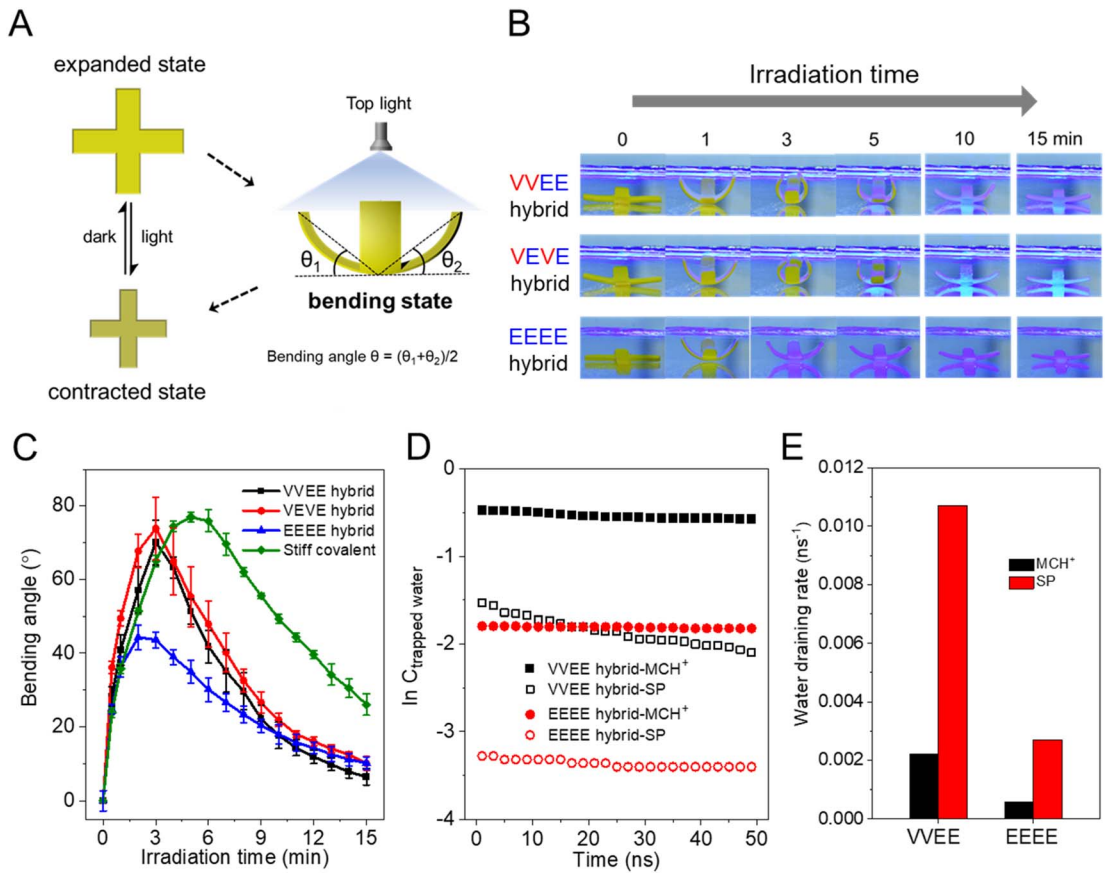

Fig. 4 (A) Schematic representation of the bending and flattening process of a cross-shaped hydrogel film containing **C1** when exposed by irradiation from the top; the bending angle was calculated as indicated on the right from photographs using ImageJ software. (B) Photographs of bending and flattening of different cross-shaped hydrogel films (0.5 mm thick) containing **C1** irradiated continuously with blue light from the top (450 nm, 120 mW cm^{-2}). (C) Plot of bending angles of PA hybrid films containing **C1** and different supramolecular nanostructures as well as stiff covalent hydrogel with a crosslinker ratio of 10%. (D) Plot of the trapped water concentration calculated from a computer simulation as a function of time for VVEE, EEEE hybrid polymers containing either the MCH^+ or SP moieties of **C1** (plotted on a logarithmic scale). (E) Plot of the fitted water draining rate for VVEE and EEEE hybrid polymers containing either the MCH^+ or SP moieties of **C1** obtained from linear fitting of the data in (D).

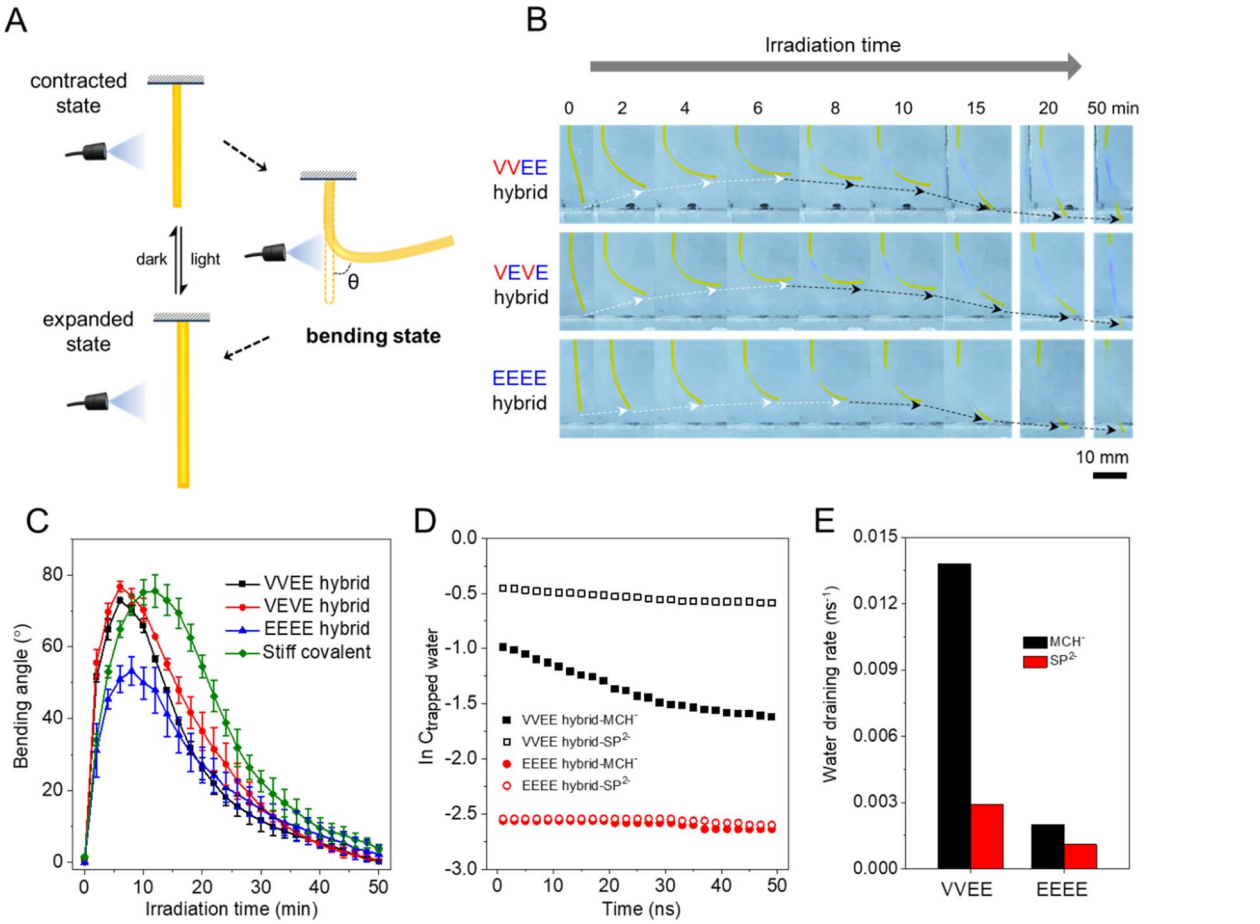

Fig. 5 (A) Schematic representation of the bending-unbending process of a rod hydrogel containing **C2** by irradiation from left. (B) Photographs of bending rod hydrogels containing **C2** upon irradiation with continuous blue light from left (450 nm, 15 mW cm^{-2}). (C) Plot of bending angles of PA hybrid hydrogels containing **C2** with different supramolecular nanostructures as well as stiff covalent hydrogel with a crosslinker ratio of 10%. (D) Time evolution of concentration of trapped water for VVEE, EEEE hybrid polymers containing **C2** obtained from simulation. (E) Fitted water draining rate for VVEE and EEEE hybrid polymers containing **C2** obtained from linear fitting of data in (D).

trapped water in different systems (see ESI† for details). As shown in Fig. 4E, the water draining rate for both the VVEE and EEEE hybrid systems increased upon irradiation, which can be explained by the hydrophobic nature of the ring-closed form of the **C1** molecule. In comparison, the water draining rates of the SP and MCH control systems are both very small (Fig. S16C and D†), which suggests a more dynamic environment for water diffusion in the hybrid materials containing supramolecular polymers relative to samples composed only of covalent polymers. Furthermore, the presence of a high-aspect-ratio supramolecular morphology (VVEE) resulted in a much faster draining rate for trapped water in the hybrid systems for both the MCH^+ and SP forms relative to the EEEE hybrid system containing spherical micelles. To show more intuitively how the trapped water can escape from the hybrid systems, we also plotted the pathways of those draining water molecules in different systems, as shown in Fig. S17 and S18.† These indicate that the high-aspect-ratio supramolecular morphology plays a critical role in enabling the trapped water to escape from the polymer network. The results suggest that the high-aspect-ratio filaments form a more continuous, percolating structure that facilitates the channeling of water molecules out the material as a more hydrophobic environment forms upon light exposure. In contrast, spherical micelles are isolated structures with poor continuity to be effective at expelling water through long range diffusion and this way impeding mechanical actuation. We also plotted the final concentration of the trapped water for different systems and found it to be on the order of $\sim 10^{-1}$ M (Fig. S19†), which is comparable to that reported previously for other covalent polymer systems.[52] The final concentration of trapped water in the SP form is smaller than that of the MCH^+ form for all the systems investigated here. This suggests that much of the water is expelled from the hydrogel upon irradiation, which is consistent with the light-induced contraction behavior observed experimentally.

Effect of supramolecular morphology on photo-expansion of the C2 hydrogels

We found that cross-shaped **C2** hydrogels tend to display an asymmetric and unstable bending geometry upon irradiation from the bottom, probably due to non-uniform expansion of the

gel or non-specific interactions between the gel and the glass substrate. To improve the stability and reproducibility of the expanding the **C2** gels, we utilized rod-shaped hydrogel samples that hanging vertically to test the photo-expansion performance with irradiation from the left (Fig. 5A). These rod hydrogels initially bent away from the light source because of an expansion gradient across their diameter and becoming straight again with prolonged irradiation as the expansion gradient becomes smaller (Fig. 5B). The bending angles plotted in Fig. 5C revealed that the hybrid systems with a high-aspect-ratio supramolecular morphology (VVEE and VEVE) showed a larger bending angle and faster bending relative to the hybrid system with the spherical micelle supramolecular morphology (EEEE) or the fully covalent control system with low modulus. On the other hand, the stiff covalent control with a higher crosslinking density displayed a similar maximum bending angle to the VVEE and VEVE hybrids but the bending is much slower (Fig. S20†). This trend agrees with what we observed in the photo-contraction of **C1** hydrogels, indicating that the supramolecular high-aspect-ratio structures play a critical role in facilitating water diffusion, regardless of whether the water is diffusing out of the material (**C1** system) or being absorbed by the material (**C2** system) as a result of irradiation. As previously explained, we hypothesize this is due to the water permeability of supramolecular high-aspect-ratio filaments combined with their ability to create a continuous path for water diffusion as a result of their high-aspect-ratio.

To better understand the mechanisms associated with the photo-expansion and bending behaviors we observed above, we performed CG simulations and tracked the escape of water trapped in the polymer network containing **C2** (Fig. 5D). The final concentration of trapped water is larger in the SP^{2-} form than in the MCH^{-} form for all the four systems (Fig. S21†), suggesting the occurrence of a light-induced expansion that matches well with our experimental observations. To further quantify the water diffusion difference before and after irradiation, we calculated the draining rate of trapped water in Fig. 5D, E and S22,† which indicates that all four systems display a clear decrease in the draining rate of trapped water upon irradiation ($MCH^{-} \rightarrow SP^{2-}$). We interpret this decreased draining rate to be the result of the more hydrophilic nature of polymers containing the SP^{2-} moiety relative to the MCH^{-} moiety since the higher charge density of SP^{2-} makes it more difficult for water to escape. Meanwhile, we observed that the presence of the high-aspect-ratio supramolecular morphology in the VVEE hybrid resulted in a larger draining rate of trapped water in both MCH^{-} and SP^{2-} forms relative to the micelle-containing EEEE hybrid and covalent controls (Fig. 5E and S22†). We again plotted the pathways of draining water in different systems, as shown in Fig. S23 and S24.† These observations suggest that the draining rates of water trapped in VVEE hybrid polymer are the fastest in the **C2** system, highlighting the important role of the high-aspect-ratio supramolecular morphology in facilitating photo-expansion of the supramolecular-covalent hybrid polymers. Together with the previous photo-contracting **C1** system, one can conclude that the supramolecular high-aspect-ratio morphology we described here facilitates water diffusion bidirectionally, that is, both into and out of the polymer network.

Conclusions

Integration of porosity and channels into hydrogels to facilitate water diffusion has been reported to improve the actuation magnitude and speed. Previous methods to create channeled hydrogels have focused on sacrificial templates and micromolding techniques, as well as 3D printing, among others.[53] In this work, we have been able to incorporate supramolecular components of varying morphologies into photo-responsive spiropyran covalent networks to investigate their effect on mechanical reinforcement and photo-actuation of the hybrid materials. High-aspect-ratio supramolecular peptide amphiphile assemblies reinforced the hybrids and improved their light driven actuation relative to those containing spherical micelles. This trend was similar in both photo-contracting and photo-expanding systems. Based on our simulations, we conclude that the hydrophilic supramolecular high-aspect-ratio filaments are able to entangle with the covalent polymer network and increase the transport of water in and out of the hybrid materials, thus enhancing the mechanical properties and photoactuation rate. Further improvements on mechanical actuation might be possible with more precise variation of supramolecular morphology which may involve alignment or more complex structures of the water-transporting vasculature.

Data availability

The data that support the finding of this study are available in the main text and the ESI.†

Author contributions

C. L. and Q. X. contributed equally to this work. C. L. carried out the synthesis and experimental characterization. Q. X. performed the simulations. T. D. C. carried out the Cryo-TEM. H. S. carried out X-ray scattering. Y. Y. and M. H. S. performed AFM. A. I. helped with the simulations. C. L., L. C. P., G. C. S., and S. I. S. supervised the research.

Conflicts of interest

The authors declare no competing financial interest.

Acknowledgements

This work was supported by the Center for Bio-Inspired Energy Science (CBES), an Energy Frontier Research Center funded by the U.S. Department of Energy (DOE) Office of Basic Energy Sciences (DE-SC0000989). C. L. acknowledged the support from University of Science and Technology of China (KY2060000188, KY2060000212) and Natural Science Foundation of Anhui Province (2208085MB27). This work made use of the MatCI Facility which receives support from the MRSEC Program (NSF DMR-1720139) of the Materials Research Center at

Northwestern University, the IMSERC at Northwestern University, which has received support from the NIH (1S10OD012016-01/1S10RR019071-01A1), Soft and Hybrid Nanotechnology Experimental (SHyNE) Resource (NSF ECCS-1542205), the State of Illinois, and the International Institute for Nanotechnology (IIN). This work also made use of the BioCryo facility of Northwestern University's NUANCE Center, which has received support from the Soft and Hybrid Nanotechnology Experimental (SHyNE) Resource (NSF ECCS-1542205); the MRSEC program (NSF DMR-1720139) at the Materials Research Center; the International Institute for Nanotechnology (IIN); and the State of Illinois, through the IIN. The X-ray scattering experiment was performed at the DuPont-Northwestern-Dow Collaborative Access Team (DND-CAT) located at Sector 5 of the Advanced Photon Source (APS). DND-CAT is supported by Northwestern University, The Dow Chemical Company, and DuPont de Nemours, Inc., and APS is a U.S. Department of Energy (DOE) Office of Science User Facility operated for the DOE Office of Science by Argonne National Laboratory under Contract No. DE-AC02-06CH11357. The authors acknowledge Mark Seniw for creating schematic illustrations.

References

1 R. R. Sinden, C. E. Pearson, V. N. Potaman and D. W. Ussery, DNA: structure and function, in *Advances in Genome Biology*, ed. R. S. Verma, JAI, 1998, vol. 5, pp. 1–141.

2 J. D. Watson and F. H. C. Crick, Molecular structure of nucleic acids – a structure for deoxyribose nucleic acid, *Nature*, 1953, **171**(4356), 737–738.

3 M. A. Geeves and K. C. Holmes, The molecular mechanism of muscle contraction, in *Advances in Protein Chemistry*, Academic Press, 2005, vol. 71, pp. 161–193.

4 E. Behrmann, M. Muller, P. A. Penczek, H. G. Mannherz, D. J. Manstein and S. Raunser, Structure of the rigor actin-tropomyosin-myosin complex, *Cell*, 2012, **150**(2), 327–338.

5 Z. Yu, F. Tantakitti, T. Yu, L. C. Palmer, G. C. Schatz and S. I. Stupp, Simultaneous covalent and noncovalent hybrid polymerizations, *Science*, 2016, **351**(6272), 497–502.

6 S. I. Stupp, T. D. Clemons, J. K. Carrow, H. Sai and L. C. Palmer, Supramolecular and hybrid bonding polymers, *ISR J. Chem.*, 2020, **60**, 124–131.

7 X. S. Hou, C. F. Ke, Y. Zhou, Z. Xie, A. Alngadh, D. T. Keane, M. S. Nassar, Y. Y. Botros, C. A. Mirkin and J. F. Stoddart, Concurrent covalent and supramolecular polymerization, *Chem.–Eur. J.*, 2016, **22**(35), 12301–12306.

8 E. P. Bruckner, T. Curk, L. Dordevic, Z. W. Wang, Y. Yang, R. M. Qiu, A. J. Dannehoffer, H. Sai, J. Kupferberg, L. C. Palmer, E. Lujiten and S. I. Stupp, Hybrid nanocrystals of small molecules and chemically disordered polymers, *ACS Nano*, 2022, **16**(6), 8993–9003.

9 S. M. Chin, C. V. Synatschke, S. P. Liu, R. J. Nap, N. A. Sather, Q. F. Wang, Z. Alvarez, A. N. Edelbrock, T. Fyrner, L. C. Palmer, I. Szleifer, M. O. Olvera de la Cruz and S. I. Stupp, Covalent-supramolecular hybrid polymers as muscle-inspired anisotropic actuators, *Nat. Commun.*, 2018, **9**(1), 2395.

10 C. Li, A. Iscen, H. Sai, K. Sato, N. A. Sather, S. M. Chin, Z. Alvarez, L. C. Palmer, G. C. Schatz and S. I. Stupp, Supramolecular-covalent hybrid polymers for light-activated mechanical actuation, *Nat. Mater.*, 2020, **19**(8), 900–909.

11 M. Y. Guo, L. M. Pitet, H. M. Wyss, M. Vos, P. Y. W. Dankers and E. W. Meijer, Tough stimuli-responsive supramolecular hydrogels with hydrogen-bonding network junctions, *J. Am. Chem. Soc.*, 2014, **136**(19), 6969–6977.

12 K. M. Hutchins, Functional materials based on molecules with hydrogen-bonding ability: applications to drug co-crystals and polymer complexes, *R. Soc. Open Sci.*, 2018, **5**(6), 180564.

13 J. A. Neal, D. Mozhdehi and Z. B. Guan, Enhancing mechanical performance of a covalent self-healing material by sacrificial noncovalent bonds, *J. Am. Chem. Soc.*, 2015, **137**(14), 4846–4850.

14 Y. Yanagisawa, Y. L. Nan, K. Okuro and T. Aida, Mechanically robust, readily repairable polymers *via* tailored noncovalent cross-linking, *Science*, 2018, **359**(6371), 72–76.

15 H. Yang, B. Yuan, X. Zhang and O. A. Scherman, Supramolecular chemistry at interfaces: host-guest interactions for fabricating multifunctional biointerfaces, *Acc. Chem. Res.*, 2014, **47**(7), 2106–2115.

16 J. Teyssandier, S. De Feyter and K. S. Mali, Host-guest chemistry in two-dimensional supramolecular networks, *Chem. Commun.*, 2016, **52**(77), 11465–11487.

17 S. C. Huang, X. X. Xia, R. X. Fan and Z. G. Qan, Programmable electrostatic interactions expand the landscape of dynamic functional hydrogels, *Chem. Mater.*, 2020, **32**(5), 1937–1945.

18 R. M. Capito, H. S. Azevedo, Y. S. Velichko, A. Mata and S. I. Stupp, Self-assembly of large and small molecules into hierarchically ordered sacs and membranes, *Science*, 2008, **319**(5871), 1812–1816.

19 Z. M. Zhang, L. Cheng, J. Zhao, L. Wang, K. Liu, W. Yu and X. Z. Yan, Synergistic covalent and supramolecular polymers for mechanically robust but dynamic materials, *Angew. Chem., Int. Ed.*, 2020, **59**(29), 12139–12146.

20 H. Sai, A. Erbas, A. Dannenhoffer, D. X. Huang, A. Weingarten, E. Siismets, K. Jang, K. R. Qu, L. C. Palmer, M. O. Olvera de la Cruz and S. I. Stupp, Chromophore amphiphile-polyelectrolyte hybrid hydrogels for photocatalytic hydrogen production, *J. Mater. Chem. A*, 2020, **8**(1), 158–168.

21 J. Y. Sun, X. H. Zhao, W. R. K. Illeperuma, O. Chaudhuri, K. H. Oh, D. J. Mooney, J. J. Vlassak and Z. G. Suo, Highly stretchable and tough hydrogels, *Nature*, 2012, **489**(7414), 133–136.

22 C. B. Rodell, N. N. Dusaj, C. B. Highley and J. A. Burdick, Injectable and cytocompatible tough double-network hydrogels through tandem supramolecular and covalent crosslinking, *Adv. Mater.*, 2016, **28**(38), 8419–8424.

23 T. Y. Cao, H. Y. Jia, Y. C. Dong, S. B. Gui and D. S. Liu, In situ formation of covalent second network in a DNA

supramolecular hydrogel and its application for 3D cell imaging, *ACS Appl. Mater. Interfaces*, 2020, **12**(4), 4185–4192.
24 Y. C. Wang, D. Liang, Z. G. Suo and K. Jia, Synergy of noncovalent interlink and covalent toughener for tough hydrogel adhesion, *Extreme Mech. Lett.*, 2020, **39**, 100797.
25 H. Yuk, C. E. Varela, C. S. Nabzdyk, X. Y. Mao, R. F. Padera, E. T. Roche and X. H. Zhao, Dry double-sided tape for adhesion of wet tissues and devices, *Nature*, 2019, **575**(7781), 169–174.
26 B. Qin, S. Zhang, P. Sun, B. H. Tang, Z. H. Yin, X. Cao, Q. Chen, J. F. Xu and X. Zhang, Tough and multi-recyclable cross-linked supramolecular polyureas *via* incorporating noncovalent bonds into main-chains, *Adv. Mater.*, 2020, **32**(36), 2000096.
27 Z. M. Zhang, L. Cheng, J. Zhao, H. Zhang, X. Y. Zhao, Y. H. Liu, R. X. Bai, H. Pan, W. Yu and X. Z. Yan, Muscle-mimetic synergistic covalent and supramolecular polymers: phototriggered formation leads to mechanical performance boost, *J. Am. Chem. Soc.*, 2021, **143**(2), 902–911.
28 T. D. Clemons and S. I. Stupp, Design of materials with supramolecular polymers, *Prog. Polym. Sci.*, 2020, **111**, 101310.
29 G. K. Voeltz and W. A. Prinz, Sheets, ribbons and tubules – how organelles get their shape, *Nat. Rev. Mol. Cell Biol.*, 2007, **8**(3), 258–264.
30 B. Wickstead and K. Gull, The evolution of the cytoskeleton, *J. Cell Biol.*, 2011, **194**(4), 513–525.
31 R. H. Pritchard, Y. Y. S. Huang and E. M. Terentjev, Mechanics of biological networks: from the cell cytoskeleton to connective tissue, *Soft Matter*, 2014, **10**(12), 1864–1884.
32 S. O. Lie, B. H. Schofield, H. A. Taylor Jr and S. B. Doty, Structure and function of the lysosomes of human fibroblasts in culture: dependence on medium pH, *Pediatr. Res.*, 1973, **7**(1), 13–19.
33 L. Brunsveld, B. J. Folmer, E. W. Meijer and R. P. Sijbesma, Supramolecular polymers, *Chem. Rev.*, 2001, **101**(12), 4071–4098.
34 T. Aida, E. W. Meijer and S. I. Stupp, Functional supramolecular polymers, *Science*, 2012, **335**(6070), 813–817.
35 B. Qin, Z. H. Yin, X. Y. Tang, S. Zhang, Y. H. Wu, J. F. Xu and X. Zhang, Supramolecular polymer chemistry: from structural control to functional assembly, *Prog. Polym. Sci.*, 2020, **100**, 101167.
36 T. Aida and E. W. Meijer, Supramolecular polymers – we've come full circle, *ISR J. Chem.*, 2020, **60**, 33–47.
37 X. F. Ji, J. Y. Li, J. Z. Chen, X. D. Chi, K. L. Zhu, X. Z. Yan, M. M. Zhang and F. H. Huang, Supramolecular micelles constructed by crown ether-based molecular recognition, *Macromolecules*, 2012, **45**(16), 6457–6463.
38 W. Z. Yuan, H. Zou, W. Guo, T. X. Shen and J. Ren, Supramolecular micelles with dual temperature and redox responses for multi-controlled drug release, *Polym. Chem.*, 2013, **4**(9), 2658–2661.
39 J. D. Hartgerink, E. Beniash and S. I. Stupp, Self-assembly and mineralization of peptide-amphiphile nanofibers, *Science*, 2001, **294**(5547), 1684–1688.
40 M. L. Ma, Y. Kuang, Y. Gao, Y. Zhang, P. Gao and B. Xu, Aromatic-romatic interactions induce the self-assembly of pentapeptidic derivatives in water to form nanofibers and supramolecular hydrogels, *J. Am. Chem. Soc.*, 2010, **132**(8), 2719–2728.
41 C. B. Cooper, J. H. O. Kang, Y. K. Yin, Z. A. Yu, H. C. Wu, S. Nikzad, Y. Ochiai, H. P. Yan, W. Cai and Z. N. Bao, Multivalent assembly of flexible polymer chains into supramolecular nanofibers, *J. Am. Chem. Soc.*, 2020, **142**(39), 16814–16824.
42 S. Debnath, S. Roy and R. V. Ulijn, Peptide nanofibers with dynamic instability through nonequilibrium biocatalytic assembly, *J. Am. Chem. Soc.*, 2013, **135**(45), 16789–16792.
43 Y. Vyborna, M. Vybornyi and R. Haner, From Ribbons to networks: hierarchical organization of DNA-grafted supramolecular polymers, *J. Am. Chem. Soc.*, 2015, **137**(44), 14051–14054.
44 F. Garcia, J. Buendia and L. Sanchez, Supramolecular ribbons from amphiphilic trisamides self-assembly, *J. Org. Chem.*, 2011, **76**(15), 6271–6276.
45 E. T. Pashuck and S. I. Stupp, Direct observation of morphological transformation from twisted ribbons into helical ribbons, *J. Am. Chem. Soc.*, 2010, **132**(26), 8819–8821.
46 X. Y. Gao and H. Matsui, Peptide-based nanotubes and their applications in bionanotechnology, *Adv. Mater.*, 2005, **17**(17), 2037–2050.
47 T. Shimizu, M. Masuda and H. Minamikawa, Supramolecular nanotube architectures based on amphiphilic molecules, *Chem. Rev.*, 2005, **105**(4), 1401–1443.
48 T. Sendai, S. Biswas and T. Aida, Photoreconfigurable supramolecular nanotube, *J. Am. Chem. Soc.*, 2013, **135**(31), 11509–11512.
49 J. Y. Rho, H. Cox, E. D. H. Mansfield, S. H. Ellacott, R. Peltier, J. C. Brendel, M. Hartlieb, T. A. Waigh and S. Perrier, Dual self-assembly of supramolecular peptide nanotubes to provide stabilisation in water, *Nat. Commun.*, 2019, **10**, 4708.
50 M. P. Hendricks, K. Sato, L. C. Palmer and S. I. Stupp, Supramolecular assembly of peptide amphiphiles, *Acc. Chem. Res.*, 2017, **50**(10), 2440–2448.
51 C. Li, A. Iscen, L. C. Palmer, G. C. Schatz and S. I. Stupp, Light-driven expansion of spiropyran hydrogels, *J. Am. Chem. Soc.*, 2020, **142**(18), 8447–8453.
52 M. K. T. de Brito, W. R. dos Santos, B. R. D. Correia, R. A. de Queiroz, F. V. D. Tavares, G. L. D. Neto and A. G. B. de Lima, Moisture absorption in polymer composites reinforced with vegetable fiber: a three-dimensional investigation *via* langmuir model, *Polymers*, 2019, **11**(11), 1847.
53 R. Xie, W. Zheng, L. Guan, Y. Ai and Q. Liang, Engineering of hydrogel materials with perfusable microchannels for building vascularized tissues, *Small*, 2020, **16**(15), 1902838.